CrossMark

ORIGINAL ARTICLE

Numerical simulations of landslide-stabilizing piles: a remediation project in Söke, Turkey

Mehmet Rifat Kahyaoğlu[1] · Gökhan İmançlı[2] · Gürkan Özden[3] · Arif Ş. Kayalar[3]

Abstract A catastrophic landslide following a rainy season occurred in the backyard of a school building in Söke, Turkey. The landslide caused property damage and adversely affected the present forest cover. Immediately after the landslide, double-row stabilizing piles were designed and constructed based on the findings of two-dimensional (2D) finite element (FE) analyses to take an urgent precaution. To remedy the problem, pile displacements were monitored using inclinometers, and it was observed that the measured displacements were greater than the values calculated in the design stage. Accordingly, two different three-dimensional (3D) numerical FE models were used in tandem with the inclinometer data to determine the load transfer mechanism. In the first model, numerical analyses were made to predict the pile displacements, and while the model predicted successfully the displacement of the piles constructed in the middle with reasonable accuracy, it failed for the corner piles. In the second model, the soil load transfer between piles was determined considering the sliding mass geometry, the soil arching mechanism and the group interaction between adjacent piles. The results of the second model revealed that the middle piles with large displacements transferred their loads to the corner piles with smaller displacements. The generated soil loads, perpendicular to the sliding direction, restricted pile deformations and piles with less displacement were subjected to greater loads due to the bowl-shaped landslide. A good agreement between the computed pile displacements and inclinometer data indicates that the existing soil pressure theories should be improved considering the position of the pile in the sliding mass, the depth and deformation modulus of stationary soil, the relative movement between the soil and piles and the relative movement of adjacent piles.

Keywords Landslide remediation · Passive piles · Soil-structure interaction · Arching mechanism · Relative movement of adjacent piles

✉ Mehmet Rifat Kahyaoğlu
  rkahyaoglu@mu.edu.tr

  Gökhan İmançlı
  gimancli@pau.edu.tr

  Gürkan Özden
  gurkan.ozden@deu.edu.tr

  Arif Ş. Kayalar
  arif.kayalar@deu.edu.tr

[1] Department of Civil Engineering, Muğla Sitki Kocman University, 48000 Mentese, Muğla, Turkey

[2] Department of Civil Engineering, Pamukkale University, 20070 Buca, İzmir, Turkey

[3] Department of Civil Engineering, Dokuz Eylul University, 35160 Buca, İzmir, Turkey

Introduction

Turkey has mountainous regions and has been subjected to many landslides. Economic, environmental and social losses due to the landslides in the mountainous regions of Turkey continue to grow. The major factors of many landslides are the increasing development of landslide-prone areas, earthquakes, heavy rainfall and other causative factors such as uncontrolled excavations. The occurrence of slope stability problems is increased due to incorrect developmental planning and land use in the landslide-susceptible zones. Therefore, movement of earth, debris and rock mass is one of the most endangering geotechnical and environmental risks in the mountainous regions.

Over the past four decades, the utilization of cast-in-place reinforced concrete passive piles became one of the most commonly employed methods for increasing resisting forces against sliding soil masses (De Beer and Wallays 1970; Fukuoka 1977; Ito et al. 1981; Gudehus and Schwarz 1985; Fleming et al. 1994; Poulos 1995; Hong and Han 1996; Chen and Poulos 1997; Zeng and Liang 2002; Won et al. 2005). The many analyses of the loads acting on slope-stabilizing piles have led to improved slope stability analysis methods and have proposed new approaches (Poulos 1973, 1995; Ito and Matsui 1975; De Beer and Carpentier 1977; Matsui et al. 1982; Goh et al. 1997; Hassiotis et al. 1997; Cai and Ugai 2000; Pan et al. 2000, 2002; Chen 2001; Liang and Yamin 2009; Zhou et al. 2014).

Ito and Matsui (1975), in an analytical study, calculated the soil loads resulting from soil movement on piles in single row. The main assumption in their theoretical equation was that the soil was soft and able to deform plastically around the piles, while pile stiffness and the sloping ground were disregarded in their theory, which was valid only for pile spacing larger than twofold diameter. De Beer and Carpentier (1977) modified the theory of Ito and Matsui by taking into consideration variations in the principal stress directions as a function of the soil characteristics and pile spacing. The determined loads imposed by sliding cohesionless soils were considerably smaller than those calculated by Ito and Matsui; however, the estimated load difference was not significant for cohesive soils. Both methods were developed originally to determine the soil loads acting on piles with no consideration of the effects of the position of the pile on the sliding mass, the relative soil–pile and the pile–pile displacements.

The interaction between pile and soil is a fairly complex problem due to its 3-D nature, meaning that it can be influenced by the deformation properties of both the pile and soil (Chen 2001; Liang and Zeng 2002; Jeong et al. 2003; Durrani et al. 2006; Yamin and Liang 2010; Kourkoulis et al. 2011; Lirer 2012; Ashour and Ardalan 2012). The load transfer from the sliding mass to the underlying stationary soil formation requires representative models to assess the soil–pile interaction. The load transfer and its redistribution among piles should be defined as a function of soil strength, sliding soil thickness, pile spacing, relative soil–pile stiffness and the relative movement between adjacent piles; to make an accurate representation of soil loads, the existing soil load estimation methods should be improved through 3-D numerical and experimental studies.

The focus of this study is to determine the load transfer mechanism between sliding soil masses and passive piles, considering the soil–pile and pile–pile interaction. The effectiveness of slope-stabilizing piles was investigated based on both full-scale field observations and 3-D numerical back analyses, and the measured and predicted pile displacements were then compared. The analyses of the load transfer mechanism were carried out on a section of a landslide in Söke, Turkey. First, double-row passive piles were designed to stabilize the sliding soil mass and monitored during and after the construction. Monitoring of pile displacements is a commonly applied method to evaluate the performance of a piled earth retaining system. Monitoring of the passive piled retaining system for the Söke/Turkey project has been done only with inclinometer installation. Pile displacements contain the combined effects of lateral earth pressures and soil-structure interaction. The constructed piled retaining system was back analyzed by means of two different 3-D FE models based on inclinometer data. In the first model, the calculated soil loads on piles using the theories of Ito–Matsui and DeBeer–Carpentier were multiplied by the load-sharing coefficients obtained from a specifically established plane-strain FE analyses. The system was forced with these loads, and the computed and measured displacements were compared. In the second model, the as-built piled retaining system in the bowl-shaped landslide area was evaluated fully considering the 3-D and arching effects (Terzaghi 1936) to identify the loads acting on the piles. This paper includes the results of a research effort in the range of a comprehensive case study.

Investigation of soil properties and landslide mechanism

The case area is located near an under-construction high school building in Söke, Turkey. The area had been denoted as high risk on landslide hazard maps, and several landslides had occurred in the past in the district, especially following rainy seasons, leading to substantial economic losses. The excavation work for the school disturbed the delicate balance and contributed to a catastrophic landslide. The landslide occurred in the backyard of the school building. It caused economic and socioeconomic losses, and impacted the natural environment. The total affected area is approximately 10,000 m^2. The school building was damaged due to the landslide and it was closed for 1-year period. This incident caused major socioeconomic impacts on students and their parents. The landslide also adversely affected the present forest cover extending behind the backyard area of the school.

Previous researches mapping the general geological formation of the study area stated that the base rock is Paleozoic age metamorphic mica schist and marble rocks belonging to the Menderes Massif. The Neogene sedimentary strata, comprising alternating units of siltstone,

claystone and sandstone unconformably cover the metamorphic base rock in the west and north of Söke (Genc et al. 2001). Soil profile on Neogene geological formations is shown in Fig. 1.

Geotechnical site investigations were carried out in order to identify the mechanism of the landslide. In addition to geotechnical studies that utilized eight engineering boreholes, geophysical studies (i.e., seismic refraction and electrical resistivity) were also carried out. The slide area including the locations of the geotechnical (BH1 to BH8) and geophysical (Profile I to Profile III) investigations is mapped in Fig. 2.

The data collected from the site investigations revealed that the slide material consists of brown, gray–yellow and gray–white clayey and silty sand, ranging from 4.5 to 10.0 m in thickness. This variation explained the three-dimensional bowl-shaped geometry of the sliding wedge, and the geophysical investigations also provided a similar geometry. Primary (P) and shear (S) wave velocities were measured as 397 and 195 m/s at the upper sliding strata, respectively. The borehole logs plotted on the electrical resistivity tomography are shown in Fig. 3.

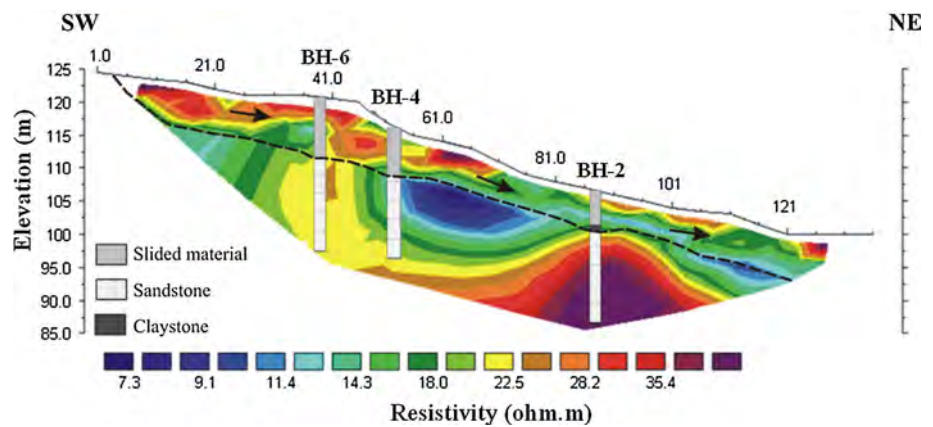The S-wave velocity was measured as 719 m/s at the lower stratum, identified as sandstone, which was also

Fig. 1 Geology and location map of the study area (Kıncal and Koca 2009)

Fig. 2 Borehole locations and geophysical profile
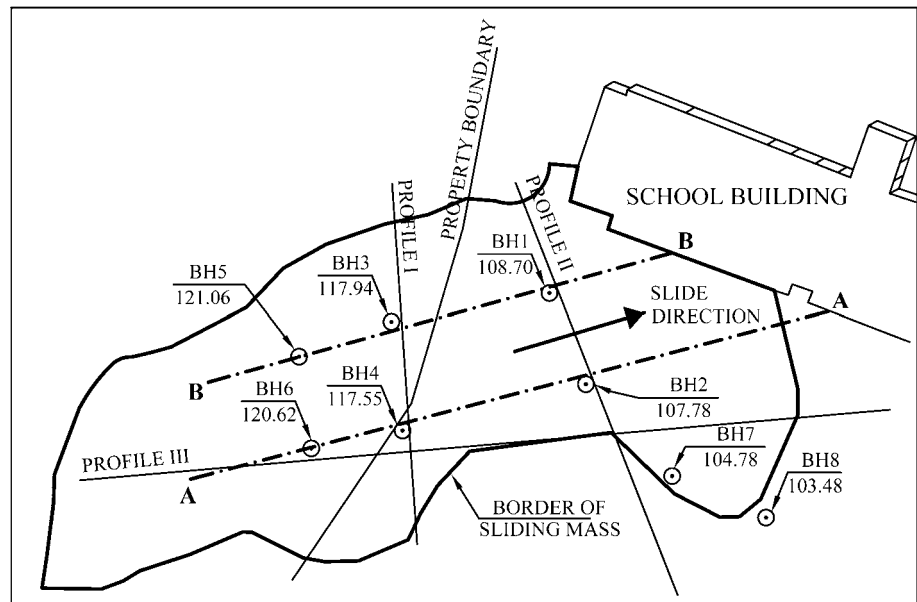
Fig. 3 Electric resistivity tomography for Profile III

subjected to unconfined compression tests and ultrasonic velocity tests. The weighted average of the unconfined compression strength was determined as 20 MPa. The minimum and maximum P-wave velocity was measured as 1775 and 3222 m/s, respectively, and the weighted average value of the P-wave velocity was calculated as 2583 m/s. Young's modulus of sandstone was calculated using P- and S-wave velocities, with the minimum, maximum and weighted average values determined as 600, 1000 and 900 MPa, respectively.

The locations of failure circles were determined based on the findings of the boreholes and geophysical tomographies. A back analysis of the failed slope was carried out to evaluate the critical shear strength parameters on the shear zone using a strength reduction technique. The value of the shear strength parameter providing the limit factor of safety against sliding was determined as $\phi_r = 13°$ for both sections, which was the same as the average value of the residual friction angle determined through direct shear

tests. Two different cross sections of the ground surface were drawn related to the topographic maps to show the situation before the excavation, after the excavation and after the slide (section A–A and section B–B in Fig. 2).

The characteristic design parameters of the sliding mass, sandstone and shear zone are summarized in Table 1.

Remediation of landslide with passive piles

Numerous slope stability analyses were carried out to identify the most appropriate remediation method considering the pile socket length and the equipment capacity of the local contractors. Based on the results, double-row piles connected by a single continuous rigid pile cap along Profile II were selected for the remediation project (Fig. 2).

Two-dimensional finite element analyses were carried out for the design of the piled retaining system. The idealized plane strain soil profile comprised three zones:

Table 1 Determined characteristic design parameters of soil layers

Soil layer	γ_{sat} (kN/m^3)	c'/c_r (kN/m^2)	ϕ'/ϕ_r (°)	V_p (m/s)	V_s (m/s)	E'/E_r (kN/m^2)	υ
Sliding mass (effective)	20	5	18	397	195	10,000	0.30
Shear zone (residual)	20	0	13	–	–	5000	0.30
Sandstone (effective)	20.5	200	36	2583	719	900,000	0.35

sandstone at the bottom, the sliding mass at the top and a thin layer of soil (residual shear zone) in between. The Mohr–Coulomb soil model was utilized in line with the effective stress parameters of the soil layers, and the respective soil model is given in Fig. 4.

A piled retaining system comprising 49 double-row cast-in-place reinforced concrete piles was designed following 2-D numerical analyses. The required embedment length to provide passive resistance at the base rock was 8.0 m, and the total pile length was 15 m. The diameter of each pile was 120 cm, and the pile rows were connected with an 80-cm-thick rigid pile cap. Pile center-to-center spacing was 2.4 m (S = 2B), with a center-to-center spacing of the pile rows of 3.15 m. A groundwater drainage system (horizontal drains) comprising 12 drilled drains, each of which was 20 m long and parallel to the base rock in two rows, was also designed to prevent pore water pressure accumulation during rainy seasons. The center-to-center spacing between the individual drains was set at 4.8 m. A cross-sectional view of the designed piled retaining system is given in Fig. 5.

Based on the results of the plane-strain analyses of the designed system, the maximum pile-head deflection was calculated as 3.5 mm. In the construction stage, the designed socket length was not achieved for all piles at the site due to the inadequate pile-drilling capacity, and so there were differences between the constructed and the designed system. As-built pile lengths in Söke project are quite variable. The range of constructed pile lengths is 9.2–14.7 m, and the range of rock socket lengths is 5.5–13.0 m. Total pile lengths, rock socket lengths and embedment ratio (socket length/total length) are given in Table 2. In this table, total pile length is the length from the bottom of the rigid pile cap to the toe of the pile.

In order to assess the performance of the constructed retaining system, four piles (Pile #9, Pile #19, Pile #27 and Pile #38 in Fig. 6) were fitted with inclinometer casings in the center of the pile shafts that would allow the pile deformations following the removal of debris material to be measured. The inclinometer data were then used in 3-D back analyses of the piled retaining system.

The 100-mm-diameter inclinometer casings were socketed 5 m into the sandstone, and the first

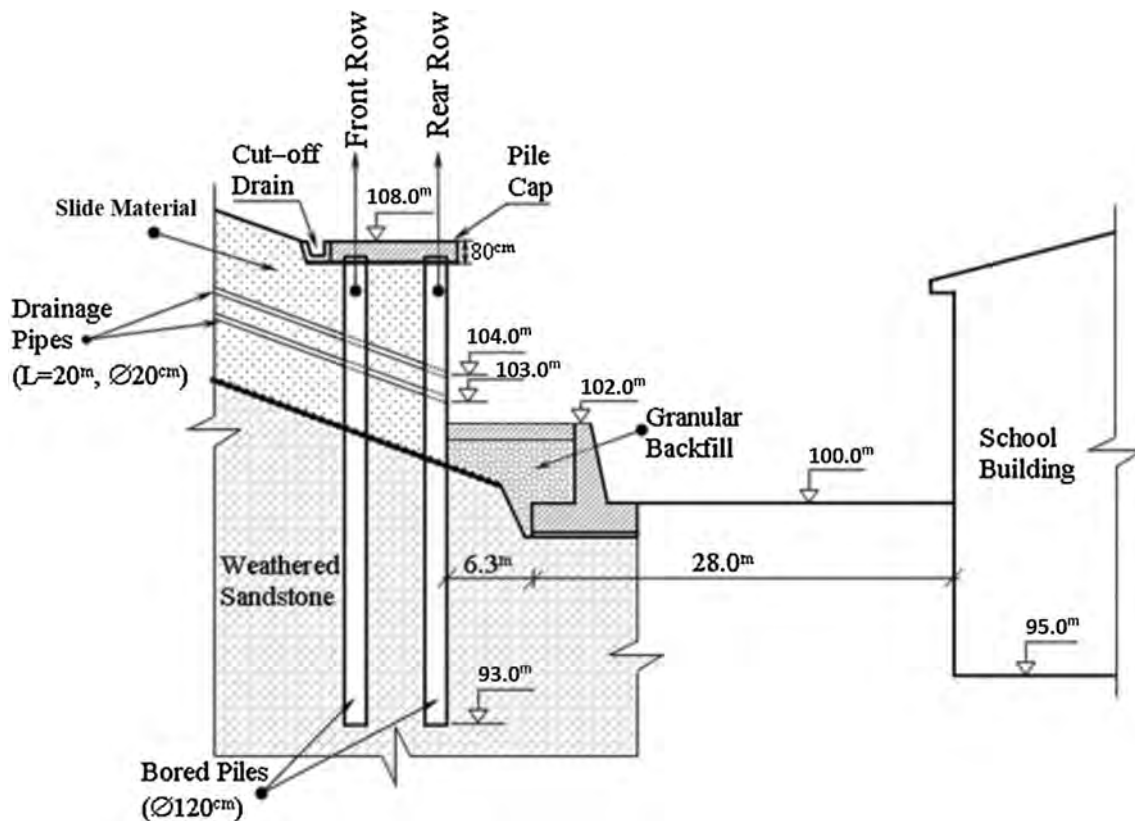**Fig. 4** Plane strain finite element soil model
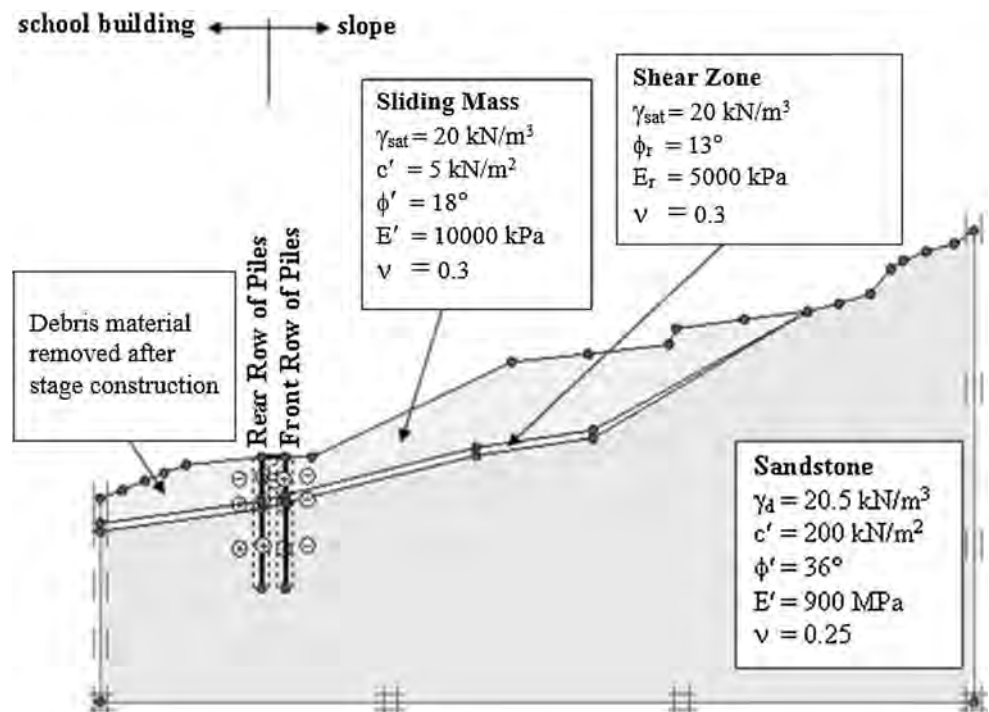
Fig. 5 Cross sectional view of the piled retaining system

inclinometer readings were recorded immediately after the completion of the piled retaining system. Subsequent readings were made upon the removal of the debris in front of the piles throughout the rainy 5-month period. The maximum pile-head deflection of the system was measured at 12.03 mm after 5 months, which was almost 3.5 times greater than the estimated maximum design value (3.5 mm). It was considered that the main reason for this unforeseen difference was the complex 3-D soil–pile interaction, and so the study was improved with 3-D numerical analyses.

Determination of pile displacements

Two different 3-D FE back analysis models were established to examine the differences between the measured and the calculated displacements and to investigate the actual soil loads acting on the piles. In the first model, the soil load acting along the portion of the pile above the sliding surface was calculated using the aforementioned theories, and the passive resistance provided from the stable portion was computed using the p–y method. The second model assessed the soil–pile interaction, with the nonlinear behavior of the surrounding soil also being taken

into consideration. The given pile lengths in Table 2 have been used in these simulations.

Determination of pile displacements using p–y and theoretical load methods

In the first model, a commercial structural analysis program (SAP2000) (Computers and Structures Inc 2011) was utilized. Soil loads were applied to the pile portion above the sliding surface, and soil–pile springs were used along the pile portion below the sliding surface. The schematic view of this 3-D FE model of the constructed retaining system is given in Fig. 7.

The equivalent subgrade moduli of soil–pile springs in the stable soil layer were also determined by means of p–y curves for weak rocks (Reese 1983; Reese et al. 1992) and inclinometer measurements. The nonlinear p–y curves were generated based on the weighted average value of RQD (40%) and the unconfined compression strength ($q_u = 20$ MPa) of the sandstone, and are shown in Fig. 8. The equivalent soil–pile springs for each meter were calculated corresponding to the field inclinometer displacements and nonlinear p–y curves of the sandstone.

The soil loads that would act on the piles were first defined according to the theories of Ito and Matsui (1975)

Table 2 As-built pile lengths

Pile no	1	2	3	4	5	6	7	8	9	10
Pile total length (m)	12.2	13.2	10.2	10.2	10.2	9.2	10.7	10.7	10.2	13.7
Rock socket length (m)	12.2	12.5	8.0	7.0	6.5	5.5	7.5	6.5	6.5	9.5
Embedment ratio (%)	100	95	78	69	64	60	70	61	64	69
Pile no	11	12	13	14	15	16	17	18	19	20
Pile total length (m)	14.2	14.2	15.2	14.2	14.7	14.2	14.2	14.2	14.2	12.2
Rock socket length (m)	10.0	10.0	11.0	10.0	11.5	10	11.0	10.5	14.2	12.2
Embedment ratio (%)	70	70	72	70	78	70	77	74	100	100
Pile no	21	22	23	24	25	26	27	28	29	30
Pile total length (m)	12.2	12.2	12.2	12.2	13.2	13.2	13.2	14.7	10.7	14.2
Rock socket length(m)	12.2	12.2	12.2	12.2	13.0	12.5	13.0	12.5	8.5	11
Embedment ratio (%)	100	100	100	100	98	95	98	85	79	77
Pile no	31	32	33	34	35	36	37	38	39	40
Pile total length (m)	10.7	13.7	13.7	12.2	12.7	12.7	12.7	12.7	10.7	12.7
Rock socket length (m)	7.5	9.5	10.5	8.5	8.5	9.5	9.0	8.5	7.5	9.5
Embedment ratio (%)	70	69	77	70	67	75	71	67	70	75
Pile no	41	42	43	44	45	46	47	48	49	
Pile total length (m)	12.7	11.7	11.7	11.7	12.2	12.2	12.2	12.2	12.2	
Rock socket length (m)	8.5	8.5	8.5	8.5	12.2	12.2	12.2	12.2	12.2	
Embedment ratio (%)	67	73	73	73	100	100	100	100	100	

and De Beer and Carpentier (1977), which were developed originally for a single pile row. The soil loads calculated for a single row of piles were shared between the first and second pile rows by the load distribution coefficients obtained from a rather comprehensive plane strain FE model. The model was capable of simulating the relative movements of the piles with respect to each other and to the sliding soil mass (Fig. 9).

In this specific simulative model, a unit load was applied to the soil on the top of the model to be displaced through the pile rows. The elastic soil with a low deformation modulus at the bottom provided the soil movement in the intended direction. The model was free to deform along the vertical boundaries (in the direction of applied load), but was constrained along the horizontal boundary (perpendicular to the applied load). The piles were hung with fixed-end anchors, and the pile displacements could be adjusted according to the measured pile-head displacements by altering the stiffness of the anchors. After providing the field pile-head displacements, the loads on the anchors were determined as the loads acting on the piles.

The dimension of the model parallel to the direction of the soil movement was finalized upon several trials until boundary effects became negligible. The soil–pile interface strength parameter was set to two-thirds of the corresponding soil strength parameter by means of the interface
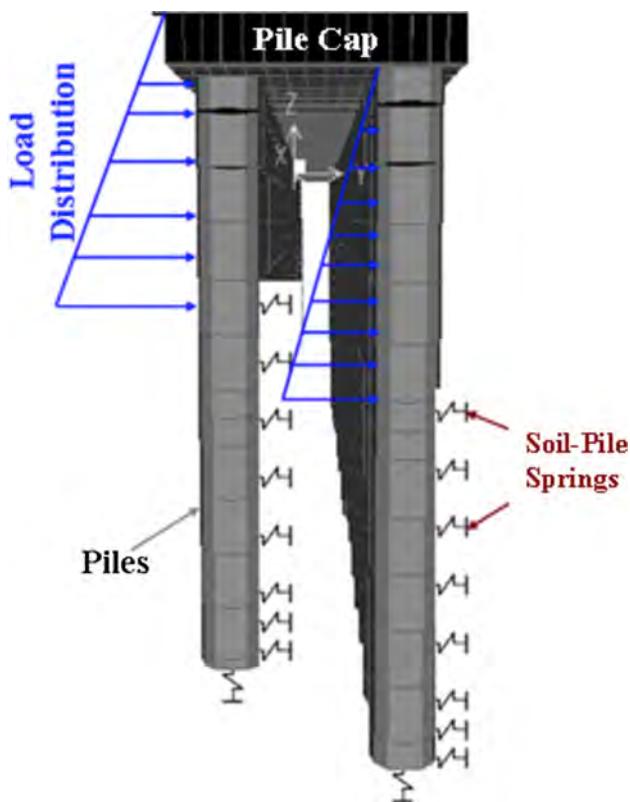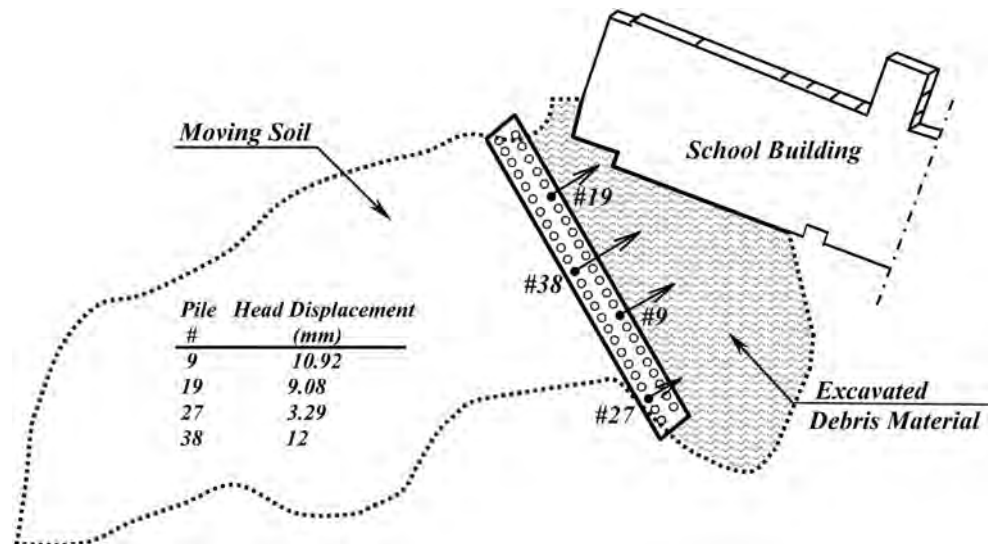
parameter (R_{inter}), so that strength reduction occurred by slippage of the soil around the pile was taken into consideration. The general characteristics of the model, including the materials and elements, are given in Table 3.

The loads acting on the front and the rear rows were determined as 56 and 44% of the applied load (P), respectively. Validity of the values of these load-sharing coefficients has been discussed in the following subsection. These values are used to determine the soil loads on the pile rows. It would appear in this case that the lateral soil pressure estimated using the approaches of Ito–Matsui and DeBeer–Carpentier needs to be adjusted by 0.56 for the front piles and 0.44 for rear piles. The calculated soil loads using the available theories of Ito–Matsui and DeBeer–Carpentier are multiplied by these coefficients and applied to the pile portion above the sliding surface.

The constructed system was analyzed with the determined soil loads and soil springs using the above-mentioned method. In the analysis, rigid pile cap and as-built socket lengths were taken into account. The computed displacements and measured displacements for Piles #9, #19, #27 and #38 are compared in Fig. 10.

In the analyses, it was interesting to note that the head displacements of Piles #19 and #38 were approximately in line with the prediction made using the theory of Ito–Matsui, while the head displacement of Pile #27 was in

Fig. 6 Pile-head deformations following the removal of debris material

Determination of pile displacements using the soil–pile–soil interaction model

It is apparent that the real pile displacements are greater than those deduced using p–y and theoretical approaches. In order to investigate this difference, which occurs due to the 3-D characteristics of the problem, the constructed piled retaining system was re-examined using a commercial finite element analyses program (PLAXIS 3D) (Brinkgreve and Broere 2006). In the analysis, the representative model was prepared considering the required number of cross sections over the entire landslide area.

The model of the constructed system with the assigned boundary conditions (bottom fixed and sides fixed in a lateral direction) is shown in Fig. 11. The construction stages of the retaining system and excavation of the debris material in front of the piles were all considered in this soil–pile–soil interaction model, and the assigned soil and material parameters are presented in Table 4.

In the soil–pile interaction analyses, the deformation modulus of sandstone varied from 600 to 1000 MPa in order to achieve the measured pile displacements (minimum, maximum and weighted average values of deformation modulus were determined as 600, 1000 and 900 MPa, respectively). While the deformation modulus of weathered sandstone was adjusted as 770 MPa, the measured and calculated displacements matched perfectly. The computed and measured displacements for Piles #9, #19, #27 and #38 are plotted in Fig. 12. For the middle piles, the load-sharing coefficients of the front and rear rows were calculated as 0.53 and 0.47, respectively, and these coefficients were determined as 0.64 and 0.36 for the corner piles. These values are not the used values, but the selectively calculated values from the data obtained in the 3-D FEM analysis. They are given to compare with the values

Fig. 7 3-D FE model of the constructed piled retaining system

line with the theory of De Beer–Carpentier. That said, both theories generated considerably smaller displacements for Pile #9. It is possible that the relatively thick sliding soil mass and the small pile socket length resulted in a greater rigid body rotation in Pile #9, and furthermore, the equivalent soil–pile springs in the model could not have represented the deformation of the pile in sandstone.
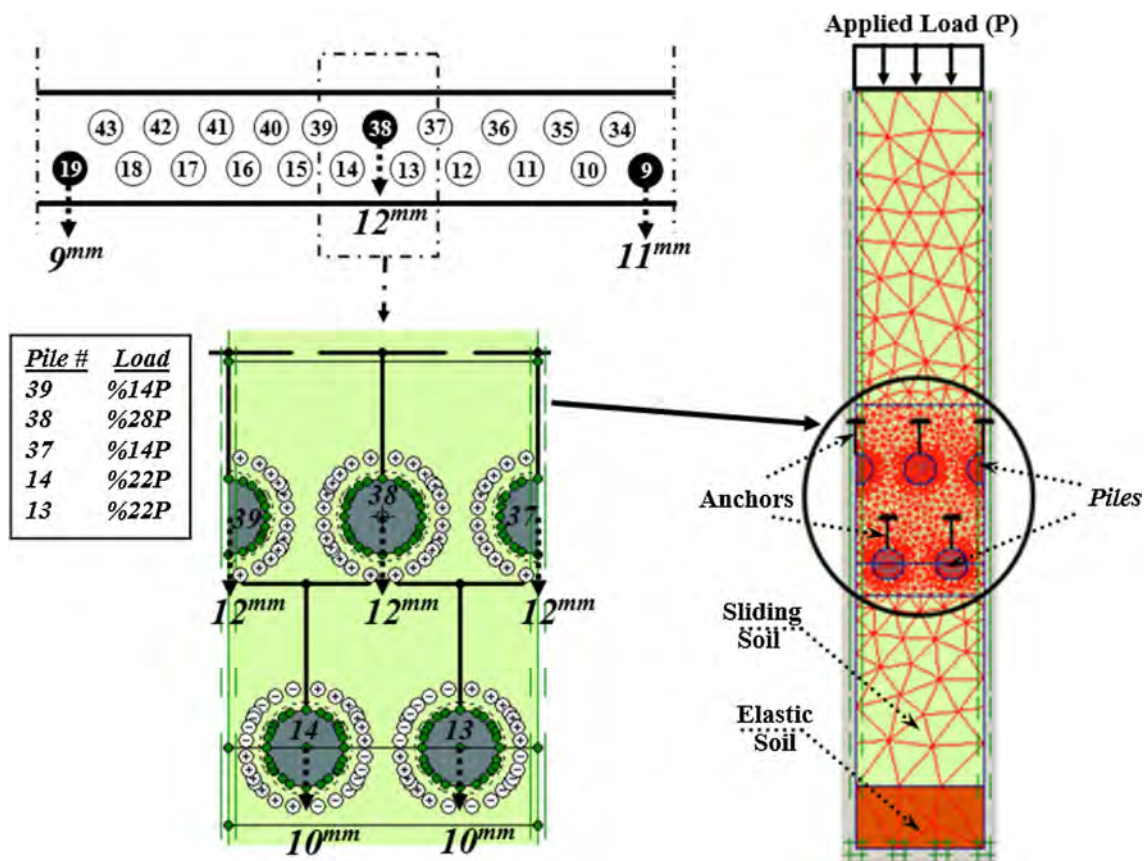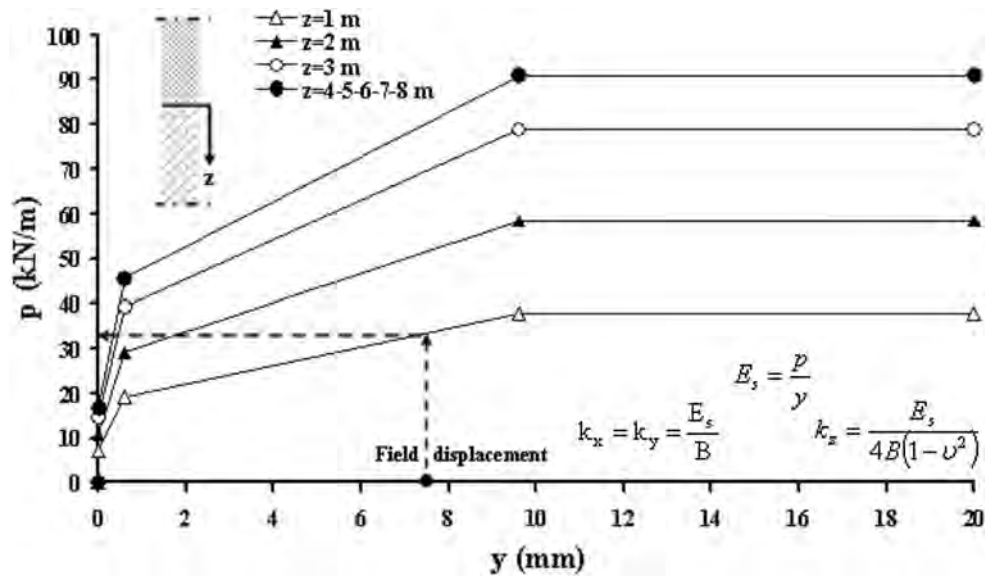
Fig. 8 Nonlinear soil–pile deformation (p–y) curves for the sandstone

$$E_s = \frac{p}{y}$$

$$k_x = k_y = \frac{E_s}{B}$$

$$k_z = \frac{E_s}{4B(1-\upsilon^2)}$$

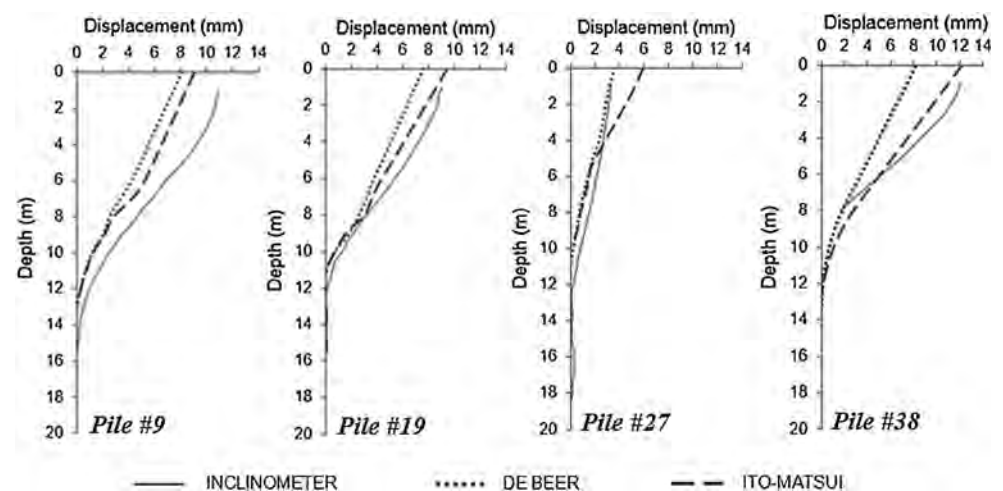| Pile #	Load
39	%14P
38	%28P
37	%14P
14	%22P
13	%22P

Fig. 9 FE model representing sliding soil and pile rows

in the preceding section. The averages of the corresponding values in this case are 0.58 and 0.43. These values are in good agreement with the values given in the preceding section which are 0.56 and 0.44.

Due to the bowl-shaped landslide geometry, a shear force was generated that was perpendicular to the direction of sliding. This shear force restricted the pile deformations, and the piles with less displacement were subjected to more soil loads in the direction of sliding. Pile #9 was subjected

Table 3 Soil and material properties in plane strain FEM analysis

	Parameter	Name	Value	Unit
Sliding soil	Material model	Model	Mohr–Coulomb	–
	Type of material behavior	Type	Drained	–
	Young's modulus (constant)	E_{ref}	10,000	kN/m^2
	Poisson's ratio	υ	0.3	–
	Effective cohesion (constant)	c'	5	kN/m^2
	Effective friction angle	ϕ'	18	°
	Dilatancy angle	ψ	0	°
	Interface roughness	R_{inter}	0.67	–
Elastic soil	Material model	Model	Linear elastic	–
	Type of material behavior	Type	Non-porous	–
	Young's modulus (constant)	E_{ref}	100	kN/m^2
	Poisson's ratio	υ	0.20	–
Pile (ϕ120)	Material model	Model	Linear elastic	–
	Type of material behavior	Type	Non-porous	–
	Young's modulus (constant)	E_{ref}	1×10^7	kN/m^2
	Poisson's ratio	υ	0.2	–
1st row anchor	Material type	Type	Elastic	–
	Rigidity	EA	Varied	kN/m
		$L_{spacing}$	1	m
2nd row anchor	Material type	Type	Elastic	–
	Rigidity	EA	Varied	kN/m
		$L_{spacing}$	1	m

Fig. 10 Computed displacements of Piles #9, #19, #27, #38 with Sap2000

to 35% higher loads than were theoretically expected (Ito and Matsui 1975; De Beer and Carpentier 1977) due to the generated shear force. The shear force effect on the load acting on piles is shown in Fig. 13.

Discussions on 3-D back analyses results

The differences between the measured and the calculated displacements of the constructed piled retaining system have been examined by two different 3-D FE back analyses. The established models also provided examination and investigation of the actual soil loads acting on the piles.

In the first analysis, lateral loads on passive piles due to the sliding soil mass above the sliding surface have been evaluated by the existing lateral soil pressure theories. The passive resistances provided by the stable portions of the piles below the sliding surface have been computed using the p–y method. The used lateral soil pressure formulations had been developed originally for a

Fig. 11 3-D model of soil–pile–soil interaction. **a** 3-D view with boundary conditions, **b** A–A section of the model, **c** B–B section of the model
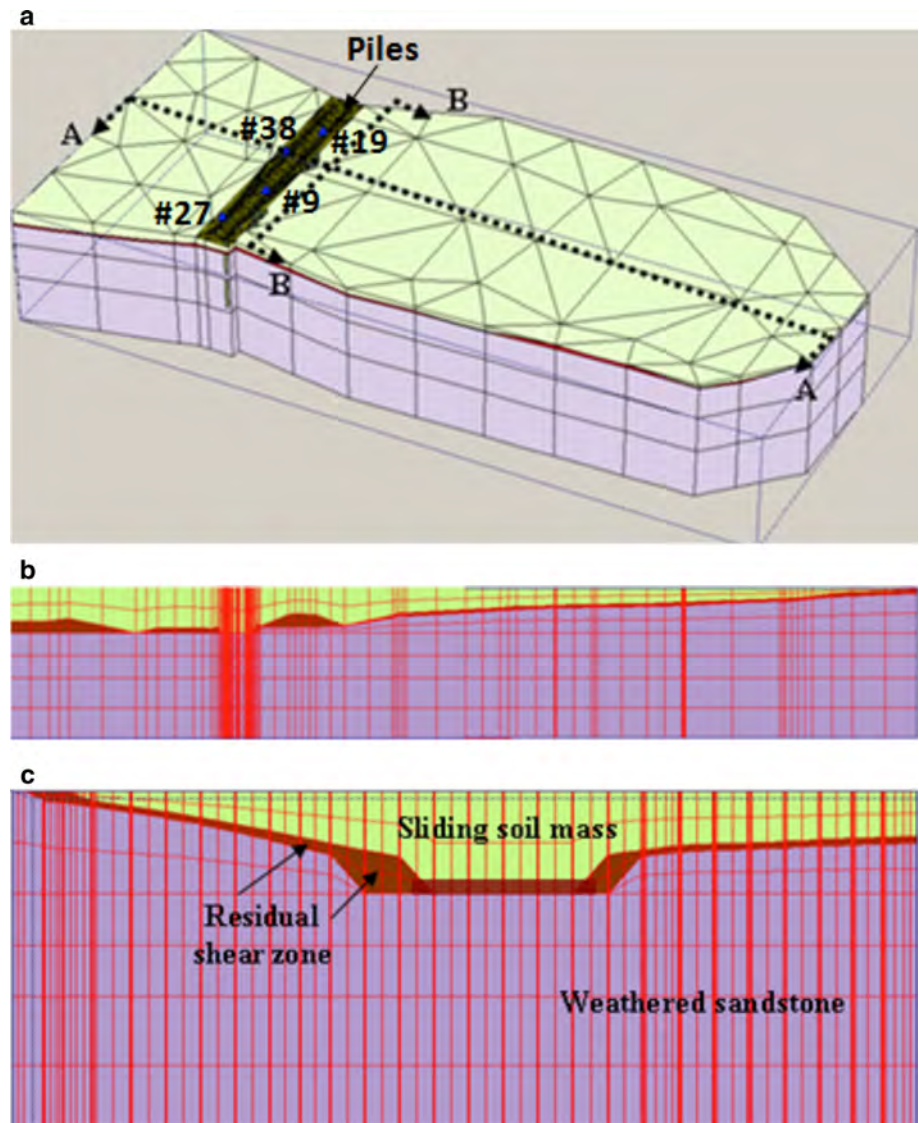
single row of piles. When these methods are applied for double rows, load sharing between the front and rear rows needs to be evaluated realistically. Determination of load sharing in classical approach is a drawback. In this paper, the values of the load-sharing coefficients for the front and the rear rows of piles have been determined by making use of an original 2-D FEM model. The model in Fig. 9 represents a slice of constant thickness soil body flowing between four piles, under the effect of an applied load. In this model, pile displacements and soil properties are controllable. As to the authors, this particular FEM solution is a simple and original approach capable of simulating the relative movements of the piles with respect to each other and to the sliding soil mass. Validity of the load-sharing coefficients obtained with this approach has been discussed in the preceding subsection. This first analysis resulted smaller pile displacements

than the real pile displacements obtained from inclinometer readings.

The second method of analysis assessing the soil–pile interaction with the nonlinear behavior of the surrounding soil resulted in a better representation of the measured pile displacements.

The displacements of the piles calculated in the 3-D back analyses are plotted together with the field inclinometer data in Fig. 14.

The results of back analyses revealed that the theoretically calculated loads and resultant loads are quite different owing to the soil arching mechanism and pile rigidity. Due to the bowl shape of the landslide, middle piles possess larger unsupported (free) lengths compared with the corner piles. In fact, most of the corner piles are totally embedded in the stable rock. Rock embedment ratios (rock socket length/total length) of the piles are given in Table 2. In this

Table 4 Soil and material properties in soil–pile interaction model analysis

Parameter	Name	Sliding soil mass	Residual shear zone	Weathered sandstone	Pile
Material model	Model	Mohr–Coulomb	Mohr–Coulomb	Mohr–Coulomb	Linear elastic
Material behavior	Type	Drained	Drained	Drained	Non-porous
Unit weight (kN/m^3)	γ	20	20	20.5	24
Young's modulus (kN/m^2)	E	10×10^3	5×10^3	9×10^5	3×10^7
Poisson's constant	υ	0.3	0.3	0.35	0.15
Cohesion (kN/m^2)	c	5	0	200	–
Friction angle (°)	ϕ	18	13	36	–
Interface reduction factor	R_{inter}	0.67	0.10	1.0	1.0
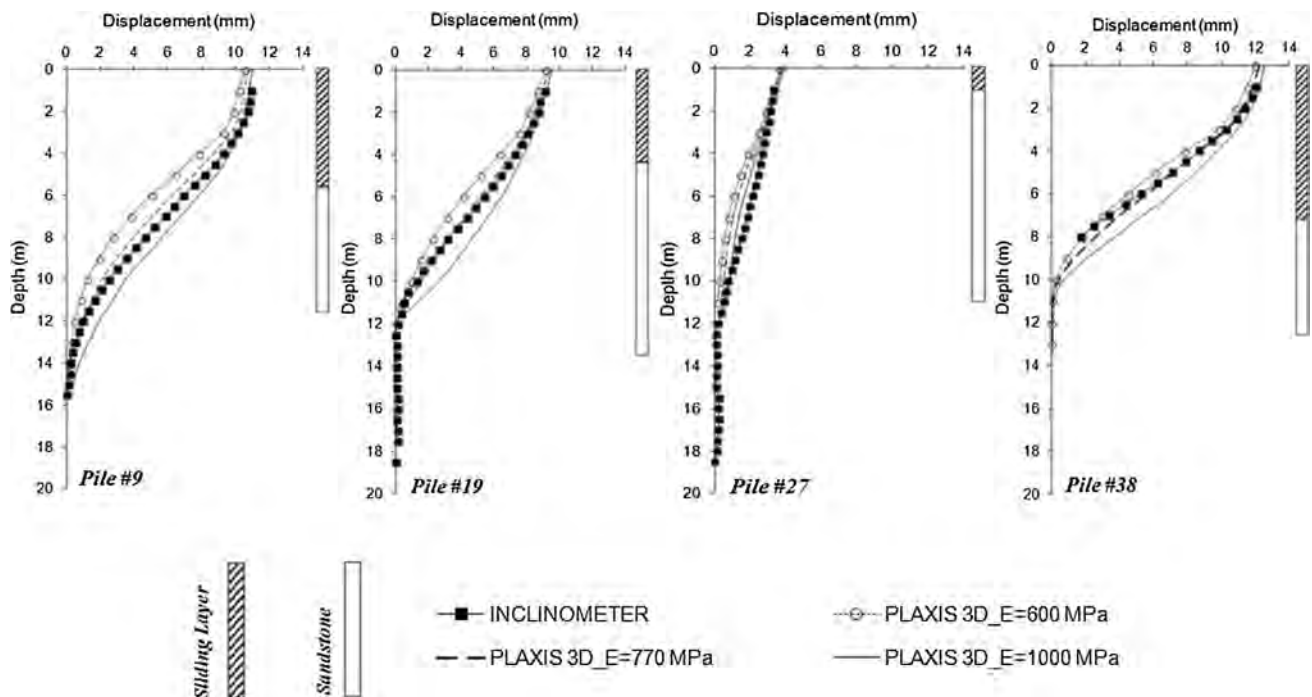
Fig. 12 Computed displacements of Piles #9, #19, #27, #38 with Plaxis 3D

table, high rock embedment ratios are related to the corner piles and low rock embedment ratios are related to middle piles. Because of the rock embedment ratio differences, lateral displacement ability of the piles is different. On the other hand, considering the shear modulus of the soil, modulus of elasticity, diameter and length of the pile, all of these piles behave as if they were infinitely long piles (Randolph 1981). The middle piles displaced more than the corner piles and transferred their loads to the corner piles. As a result of this transfer, the corner piles were subjected to more soil loads.

It is noteworthy that the load transfers to neighboring piles resulted in the attainment of lower soil loads on Piles #19 and #38, located in the center of the piled retaining system, despite of the greatest thickness of the sliding material. Contrary to common expectations, the soil loads

were lower on these piles since the loads were transferred to the piles adjacent to the edges, such as Pile #9 and Pile #27. In addition, the influence of the sliding soil depth became more pronounced as the pile length increased. For the corner piles, subjected to shallow depths of sliding, pile resistance was independent of pile length; however, for the middle piles, subjected to greater sliding depths, resistance increased significantly as the length of the pile increased.

Conclusion

The constructed double-row piles of the piled retaining system were re-examined with two different 3-D back analysis models to investigate the group interaction between adjacent piles in terms of the soil arching

Fig. 13 Soil loads on Piles #9, #19, #27, #38
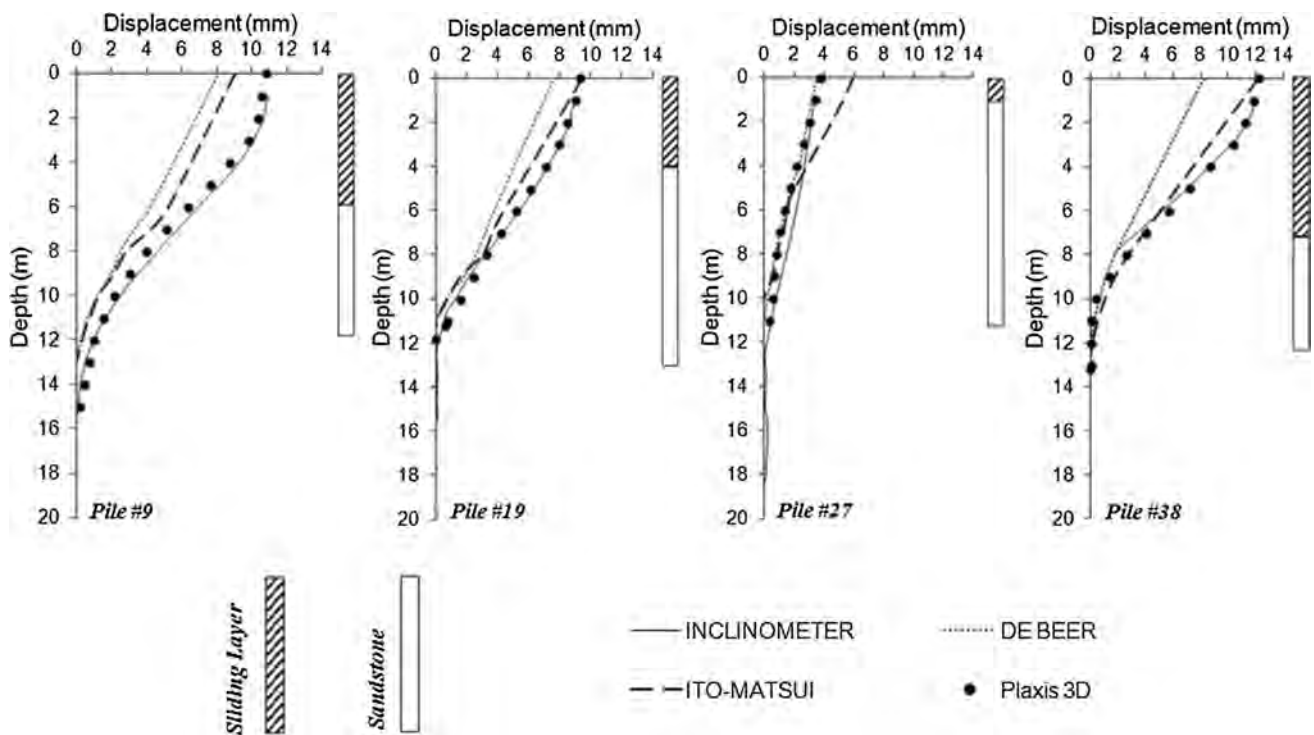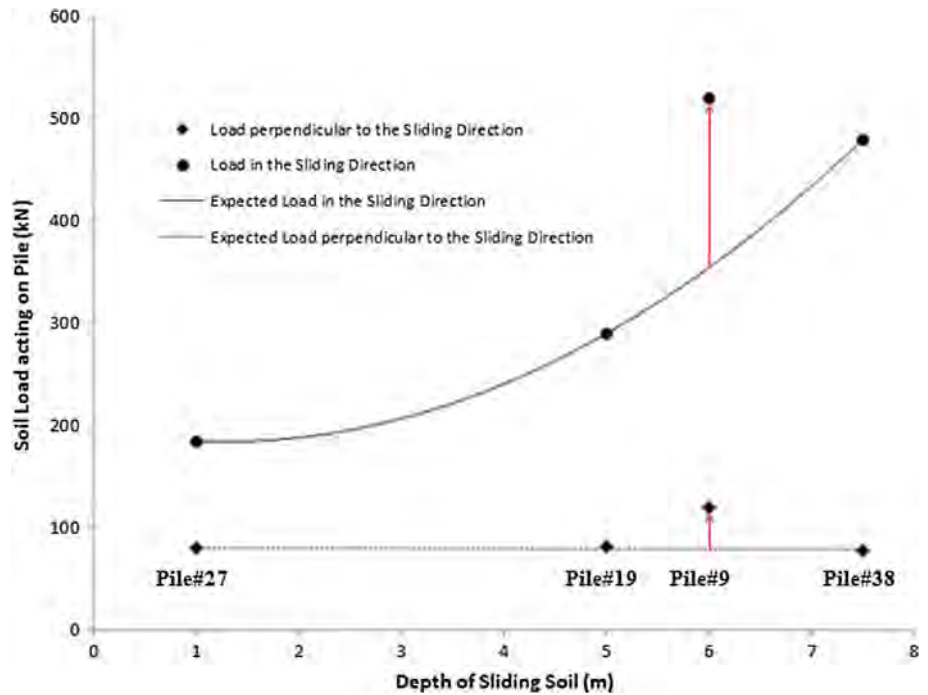
Fig. 14 Measured and computed displacements of Piles #9, #19, #27, #38

mechanism. The bowl-shaped landslide constrained the displacement of the corner piles, while the piles in the middle were free to displace due to the deep sliding mass. The middle piles displaced more than the corner piles and transferred their loads to the corner piles through soil arching.

The presented case study shows that the geometry of the sliding mass, the depth of the sliding soil, the deformation modulus of the stationary soil, the relative movement between the soil and the piles and the relative movement of adjacent piles have a combined effect on the soil loads acting on piles and pile displacements. In this regard,

existing soil pressure theories should be revisited to reconsider the arching mechanism and the position of the pile in the sliding mass.

References

Ashour M, Ardalan H (2012) Analysis of pile stabilized slopes based on soil–pile interaction. Comput Geotech 39:85–97

Brinkgreve RBJ, Broere W (2006) Plaxis 3D foundation v1.6 manual. Computers and Structures Inc. Analysis Reference Manual for Sap2000, CSI 2011

Cai F, Ugai K (2000) Numerical analysis of the stability of a slope reinforced with piles. Soils Found 40(1):73–84

Chen CY (2001) Numerical analysis of slope stabilization concepts using piles. Ph.D. thesis, The Faculty of the Graduate School University of Southern California, Los Angeles, California

Chen LT, Poulos HG (1997) Piles subjected to lateral soil movements. J Geotech Geoenviron Eng ASCE 123(9):802–811

Computers and Structures Inc (2011) Analysis Reference Manual for Sap2000

De Beer E, Carpentier R (1977) Discussions: methods to estimate lateral force acting on stabilizing piles. Soils Found 17(1):68–82

De Beer E, Wallays M (1970) Stabilization of a slope in schist by means of bored piles reinforced with steel beams. In: Proceedings of the 2th International Congress on Rock Mechanics, Belgrade, 3:361–369

Durrani JK, Ellis EA, Reddish DJ (2006) Modelling lateral pile–soil interaction for a row of piles in a frictional soil. In: 4th international FLAC symposium numerical modelling geomech, pp 231–238

Fleming WGK, Weltman AJ, Randolph MF, Elson WK (1994) Piling engineering, 2nd edn. Blanckie and Son Ltd, New York

Fukuoka M (1977) The effects of horizontal loads on piles due to landslides. In: Proceedings of the 9th international conference on soil mechanics and foundation engineering, Tokyo, Japan, pp 27–42

Genc C, Altunkaynak Ş, Karacık Z, Yazman Y (2001) The Çubukludağ graben, South of Izmir: its tectonic significance in the Neogene geological evolution of the Western Anatolia. Geodin Acta 14:1–12

Goh ATC, Teh CI, Wong KS (1997) Analysis of piles subjected to embankment induced lateral soil movements. J Geotech Geoenviron Eng 123(9):792–801

Gudehus G, Schwarz W (1985) Stabilization of creeping slopes by dowels. In: Proceedings of the 11th international conference on soil mechanics and foundation engineering, San Francisco, pp 1697–1700

Hassiotis S, Chameau JL, Gunaratne M (1997) Design method for stabilization of slopes with piles. J Geotech Geoenviron Eng ASCE 123(4):314–323

Hong WP, Han JG (1996) The behavior of stabilizing piles installed in slopes. In: Proceedings of the 7th international symposium on landslides, Rotterdam, pp 1709–1714

Ito T, Matsui T (1975) Methods to estimate lateral force acting on stabilizing piles. Soils Found 15(4):43–59

Ito T, Matsui T, Hong PW (1981) Design method for stabilizing piles against landslide—one row of piles. Soils Found 21(1):21–37

Jeong S, Kim B, Won J, Lee J (2003) Uncoupled analysis of stabilizing piles in weathered slopes. Comput Geotech 30(8):671–682

Kıncal C, Koca MY (2009) A proposed method for drawing the great circle representing dip angle and strike changes. Environ Eng Geosci 15(3):145–165

Kourkoulis R, Gelagoti F, Anastasopoulos I, Gazetas G (2011) Slope stabilizing pile and pile-groups: parametric study and design insights. J Geotech Geoenviron 137:663–677

Liang R, Yamin M (2009) Three-dimensional finite element study of arching behavior in slope/drilled shafts system. Int J Numer Anal Methods Geomech. doi:10.1002/nag.851

Liang R, Zeng S (2002) Numerical study of soil arching mechanism in drilled shafts for slope stabilization. Soils Found 42(2):83–92

Lirer S (2012) Landslide stabilizing piles: experimental evidences and numerical interpretation. Eng Geol 149:70–77

Matsui T, Hong WP, Ito T (1982) Earth pressures on piles in a row due to lateral soil movements. Soils Found 22(2):71–81

Pan JL, Goh ATC, Wong KS, Teh CI (2000) Model tests on single piles in soft clay. Can Geotech J 37:890–897

Pan JL, Goh ATC, Wong KS, Teh CI (2002) Ultimate soil pressures for piles subjected to lateral soil movements. J Geotech Geoenviron Eng ASCE 128(6):530–535

Poulos HG (1973) Analysis of piles in soil undergoing lateral movement. J Soil Mech Found Eng Div ASCE 99:391–406

Poulos HG (1995) Design of reinforcing piles to increase slope stability. Can Geotech J 32(5):808–818

Randolph MF (1981) The response of flexible piles to lateral loading. Geotechnique 31(2):247–259

Reese LC (1983) Behavior of piles and pile groups under lateral load. In: Report to the US department of transportation, Federal highway administration, Office of Research, Development, and Technology, Washington, DC

Reese LC, Wang ST, Fouse JL (1992) Use of drilled shafts in stabilizing a slope. In: Proceedings of the specialty conference on stability and performance of slopes and embankments, II, Berkeley, pp 1318–1332

Terzaghi K (1936) Stress distribution in dry and saturated sand above a yielding trap door. In: Proceedings of the 1st I.C.S.M.F.E., pp 307–311

Won J, You K, Jeong S, Kim S (2005) Coupled effects in stability analysis of soil–pile systems. Comput Geotech 32(4):304–315

Yamin M, Liang RY (2010) Limiting equilibrium method for slope/drilled shafts system. Int J Anal Numer Methods Geomech. doi:10.1002/nag.852

Zeng S, Liang R (2002) Stability analysis of drilled shafts reinforced slope. Soils Found 42(2):93–102

Zhou C, Shao W, van Westen CJ (2014) Comparing two methods to estimate lateral force acting on stabilizing piles for a landslide in the Three Gorges Reservoir, China. Eng Geol 173:41–53